TESTING METHODS FOR MEASURING THE PURE MODE III DELAMINATION TOUGHNESS OF COMPOSITE

Yangyang Ge[1], Xiaojing Gong*[1], Anita Hurez[2], Emmanuel De Luycker[1], Lingling Peng[3]

[1] Institut Clément Ader, IUT Tarbes de l'Université Toulouse III, Tarbes, France
Email: xiaojing.gong@iut-tarbes.fr

[2] Département de Recherche en Ingénierie des Véhicules pour l'Environnement, IUT Le Creusot de l'Université de Bourgogne, Le Creusot, France

[3] Département de Recherche en Ingénierie des Véhicules pour l'Environnement ISAT, Nevers, France

Keywords: Mode III delamination, Testing method, Edge Ring Crack Torsion test (ERCT)

ABSTRACT

In this work, major testing methods for characterizing the pure mode III delamination behaviors of composites are discussed and two Edge-Crack-torsion tests have been realized. Moreover, a new fracture toughness test, the Edge-Ring-Crack-Torsion method (ERCT), has been developed. This is a torsion test on a composite plate containing an edge ring crack between two layers. The loading mode obtained is pure mode III, and the distribution of G_{III} across the crack tip depends on the lay-up of the laminates used. A comparison of the two former testing methods and ERCT in terms of both experiment and modeling is presented. The importance of tests of mode III delamination is demonstrated by a comparison of the pure mode I, II and III delamination toughness.

1. Introduction

Laminate composites have a growing number of applications in the area of transport where light-weight is a main concern. These materials have valuable mechanical properties such as high specific resistance and rigidity, good resistance to impact and fatigue loading. However, their heterogeneity and anisotropy introduce computational difficulties and the defects or pores introduced by the manufacturing process are unavoidable. Moreover, damage modes of a structure in service are always very complex, especially, interlaminate fracture, named delamination, is the most common and most dangerous mode among all kinds of damages.

Delamination resistance can be expressed by a general criterion of type: $f(G_I, G_{II}, G_{III}) = 0$ by applying linear elastic fracture mechanics. A lot of attentions have been devoted to the study of pure mode I, pure mode II and mixed mode I + II. Several criteria have been proposed to describe the mixed mode I + II, such as the criteria of X.J. Gong[1] and M.L. Benzeggagh[2]. However, the generalization to mixed mode I+II+III is usually based on the hypothesis which considers identical toughness for pure mode II and mode III. In fact these two shear modes are physically independent and their critical value, G_{IIC} and G_{IIIC} can be quite different for some composites materials. Actually, the measurement of pure mode III toughness is not easy. In the literature, the most commonly used test methods should be Edge-Crack-Torsion-1[3] and 2[4] (ECT-1 and ECT-2), Modified-Edge-Crack-Torsion[5] (MECT-1) and Modified-Split-Cantilever-Beam[6,7] (MSCB) tests. Unfortunately, the participation of mode I or/and mode II in these tests can never be eliminated totally. The distribution of strain energy release rate along crack tip is far from being uniform, which is necessary to guarantee a good measurement of G_{IIIC}.

This study aims to analyze pure mode III delamination testing methods. The geometry of the specimens tested and the loading conditions has been optimized by finite element calculation. And then different testing methods have been performed. The results obtained are compared and discussed.

2.Experimental details

2.1.Material and specimens

In this study, all specimens are obtained from a woven carbon/epoxy taffeta fabric prepreg (ref: IMP503Z). Two tests proposed in the literature, ECT-1[3] and ECT-2[4], have been realized. Moreover, an original test, named Edge-Ring-Crack-Torsion (ERCT) has been performed, where the delamination is under pure mode III loading. For comparison, the toughness in pure mode I and pure mode II have also been measured.

Table 1 lists the properties of the prepreg given by the manufacturer and the stacking sequences used in pure mode III tests.

IMP503Z	ρ=200(g/m2)	Tg=120(°C)	Vf=42%
Stacking sequence for ECT-1	(45/0/0/45/0/45/45/0)/crack/(0/45/45/0/45/0/0/45)		
Stacking sequence for ECT-2 and ERCT	(0/45/45/0/45/0/0/45/45/0/0/45/0/45/45/0)/crack /(0/45/45/0/45/0/0/45/45/0/0/45/0/45/45/0)		

Table 1: Prepreg properties and stacking sequences of the laminates tested

All composite laminates are fabricated by hand lay-up technique and a polymer film of 13 μm thick is embedded in the midplan in order to create a pre-crack. For ECT specimens, the crack tip is straight and for ERCT the crack tip is circular. The composite laminates are cured in hot-press machine with a proper curing cycle.

2.2.Test conditions

A traction/compression machine and a torsion machine of MTS were used. Displacement rate was imposed to 2mm/min for ECT-1 and 0.5°/min for ECT-2 and ERCT. All tests were performed at ambient temperature. At least three specimens were tested for each method to obtain an average value.

2.3.Experimental calibration of compliance C_{exp}=f(a)

In this work, the formula of Irwin-Kies[8] (equation (1)) is applied to determine the strain energy release rate under pure mode I, pure mode II and pure mode III loadings, where P is the load, C is the compliance, B is the width and a is the initial crack length

$$G = \frac{P^2}{2B}\frac{dC}{da} \quad (1)$$

In order to apply the formula, compliance calibration is necessary and the experimental method is preferred in the ECT tests. The step is as below:

1.Make a series of test specimens of the same geometry except for different initial crack length;

2.Measure the compliance of each specimen: $C_i = V_i/P_i$ (Displacement/load) on the linear domain (see Figure 1-(a));

3.Interpolate these measured C_n as a function of the crack length to determine the compliance law: C = f (a) (Figure 1-(b));

4.Determine strain energy release rate by the Irwin-Kies formula. When P reaches P_c the critical loading, then G equals G_c.

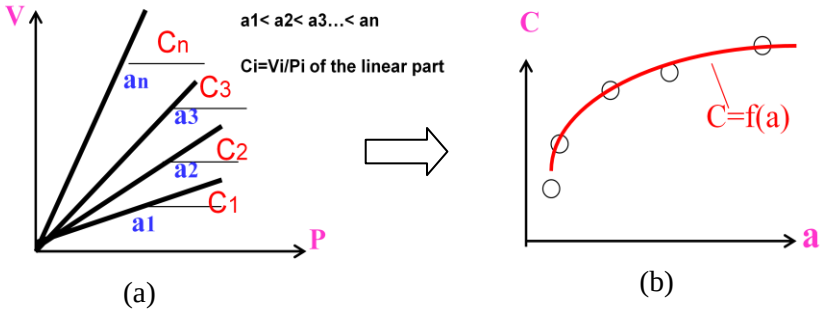

Figure 1: Experimental calibration of compliance

2.4. Mechanical properties of the composite tested

A series of tensile tests have been carried out to in order to measure material constants needed in the numerical simulation. The result is shown in Table 2.

Longitudinal and transverse modulus	55250 MPa
Tensile strength in direction 1 and 2	669 MPa
Poisson's ratio	0,044
Shear modulus in direction 12	4062 MPa
Shear stress at break in direction 12	117 MPa

Table 2: In-plane mechanical properties of woven carbon/epoxy composite

Other constants were defined according to information provided by the manufacturer and from the literature.

3. Numerical simulation

The numerical models are established in LS-Dyna. The fixtures and specimens are modeled by 3D solid elements. Spring elements are arranged along the crack tip in order to obtain forces at the crack tip. Several material models have been applied to simulate the composite specimen, and MAT 59 is chosen due to its better performance and appropriate mechanical criterion (Maximum Stress Failure Criterion). Then the virtual crack closure technique (VCCT) [9,10] is performed to determine the distribution of G_I, G_{II} and G_{III} along the crack tip (Figure *2*). This method uses the stress/nodal forces ahead of the delamination front and the displacements behind the crack tip to determinate the energy release rate components. A formula for calculating the strain energy release rate components for three dimensional eight-nodes solid components

$$G_I = \frac{F_{zj}\delta_{zj}}{2\Delta a \Delta y} \tag{2}$$

$$G_{II} = \frac{F_{xj}\delta_{xj}}{2\Delta a \Delta y} \tag{3}$$

$$G_{III} = \frac{F_{yj}\delta_{yj}}{2\Delta a \Delta y} \tag{4}$$

(See Figure 2) where Δy is half the sum of element lengths in y direction on either side of the considered node, Δa is the element length in x direction, F_x, F_y and F_z are the forces at crack tip measured on the springs elements arranged at crack tip.

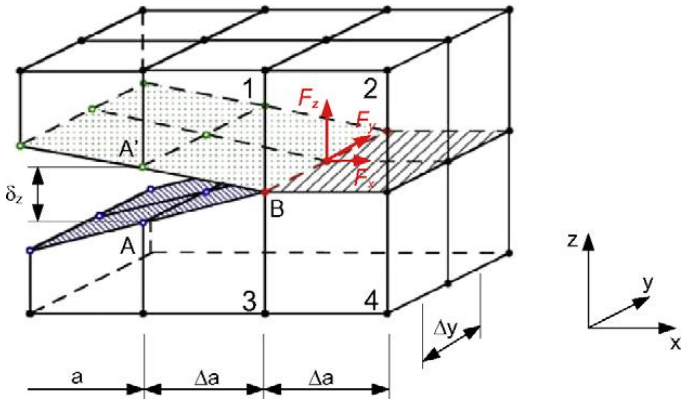

Figure 2: VCCT for three dimensional eight-nodes solid elements[11]

4.Results and discussions

4.1.ECT-1

First of all, we made a series of tests ECT-1 using the fixture shown in Figure 3 and obtained the relationship between C and a/B by experimental compliance calibration.

Figure 3: ECT-1 test

Then we applied a modified Irwin-Kies formula (Equation (5)) to calculate G_{IIIC}, where P_c is the load at the end of the linear domain in the load-displacement curve, which corresponds to the onset of crack growth.

$$G_{IIIC} = \frac{mcP_c^2}{2BL\left(1-m\left(\frac{a}{B}\right)\right)} \quad (5)$$

The results are shown in Table 3.

Specimen	P_C (N)	G_{IIIC} (N/m)
2-1	899	1218
2-2	949	1351
2-3	940	1362
Average	929	1310
Standard deviation	-	80

Table 3: Critical load measured by ECT-1 test and calculated G_{IIIC}

ECT-1 test has been simulated numerically by finite element method (Figure 4).

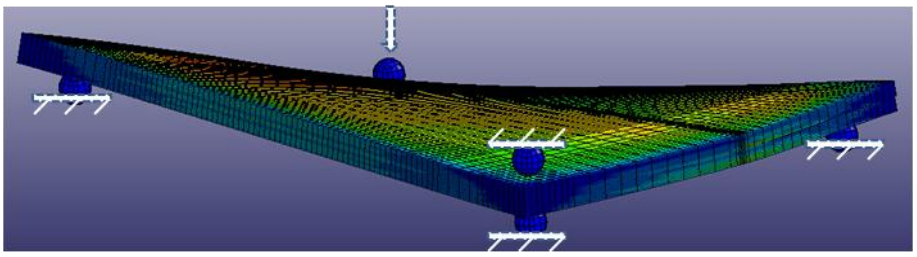

Figure 4: Model of ECT-1test

The energy release rates along the crack tip (Figure 5) were calculated by VCCT method. One can see that the distribution of G_{III} is not uniform at all, and the experimental average value obtained by equation (5) is 30% larger than the numerical one. Moreover, the mode II is very important at the edges of the crack. We can see also the participation of mode I at one edge of the crack that is significant enough to affect the delamination behavior.

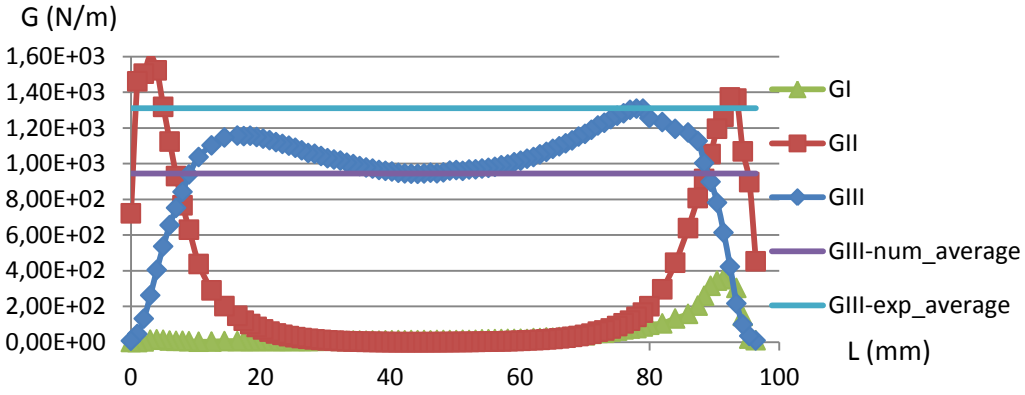

Figure 5: Evolution of G_I, G_{II} and G_{III} along the crack tip in ECT-1 test

If the single loading at the corner of the specimen is replaced by a pair of loading at two diagonal corners evenly (shown in Figure 6), we have the test named Modified-Edge-Crack-Torsion[5] (MECT-1).

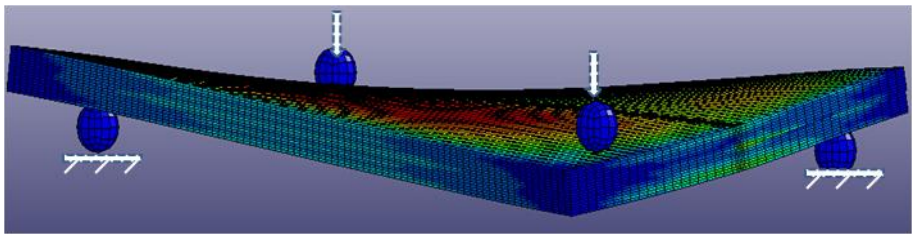

Figure 6: Model of Modified ECT test

Figure 7 shows the distribution of G_{III} in MECT-1 test. A significant improvement can be observed. The participation of mode I is nearly cancelled and in the central part mode III is constant and highly preponderant while mode II is the main mode at the two ends of the specimen. But the concern is that the maximum of G_{II} at the edges is 30% higher than that of G_{III} at the central part. This means that the delamination can be initiated at the edges controlled by mode II instead of mode III. Note that the difference between experimental and numerical average value is not really improved. The realization of this test is on the way; the results will be discussed in a future paper.

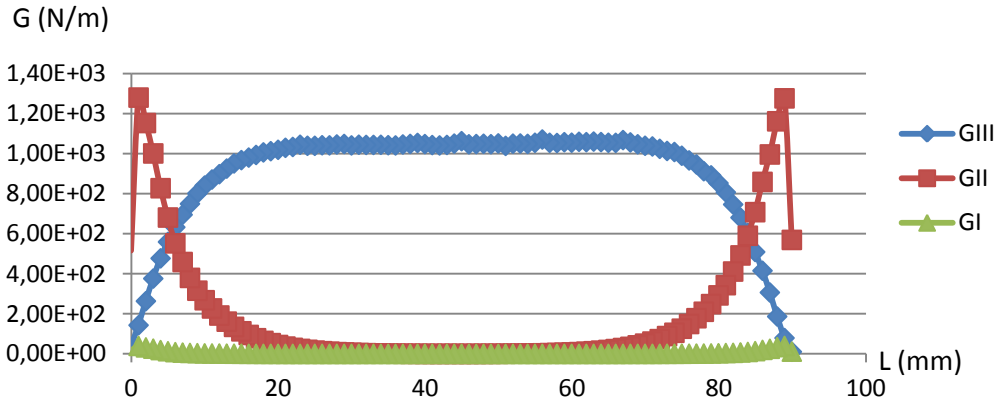

Figure 7: Evolution of G_I, G_{II} and G_{III} along the crack tip in the MECT-1 test

4.2.ECT-2 test

ECT-2 test uses a torsion machine. Both ends of specimens were loosely fixed by steel blocks in order to release the axial slide during the application of torque. This test has been carried out in our study. Figure 8 illustrates the evolution of measured torque versus rotation angle.

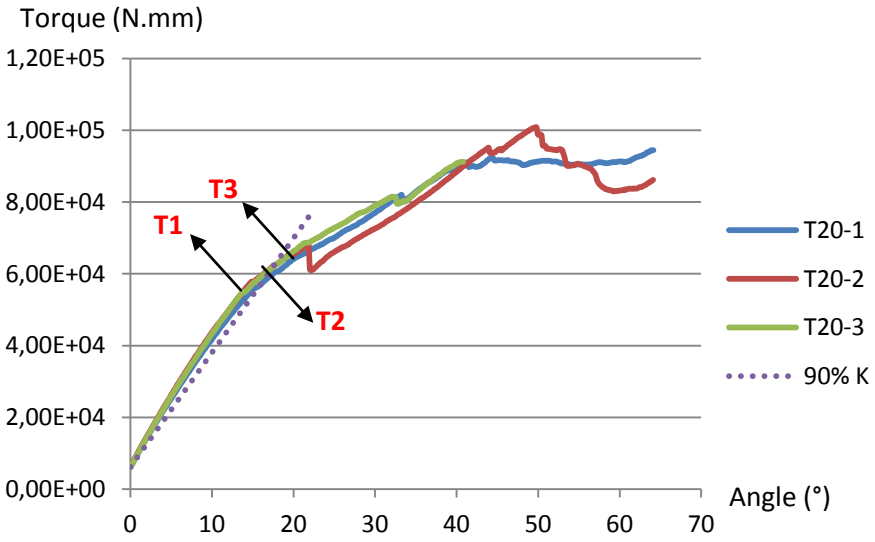

Figure 8: Experimental curves torque vs angle of ECT-2 test

The strain energy release rate was calculated according to equation (6), which is modified from equation (1)

$$G_{IIIC} = \frac{mcT^2}{2LB\left(1-m\left(\frac{a}{B}\right)\right)} \tag{6}$$

The problem shown in Figure 8 is that the critical load corresponding to crack initiation is not easy to define. Three kinds of G_{IIIC} were calculated according to different definition of T_C (Table 4): T_{C-1} denote the torque at the end of the linear domain; T_{C-2} the torque at the intersection of the curve and a line at 90% of initial slope of linear part; T_{C-3} the torque at first visible drop of the load. The deviation of G_{IIIC-3} measured on different initial crack length (10mm-25mm) looks very important. Actually, G_{IIIC-3} should not correspond to the crack initiation, but to first instable crack propagation.

	N°	T_{C-1} (N.mm) (linear end)	T_{C-2} (N.mm) (90% K)	T_{C-3} (N.mm) (visible drop)	G_{IIIC-1} (N/m)	G_{IIIC-2} (N/m)	G_{IIIC-3} (N/m)
Geometry 1	T10-1	66776	67051	76139	1007	1016	1310
	T10-2	68325	71045	76827	948	1025	1199
Geometry 2	T15-1	57481	60490	70563	954	1057	1438
	T15-2	56552	59254	65607	845	927	1137
Geometry 3	T20-1	55657	56802	82026	929	967	2017
	T20-2	57619	59298	68050	944	1000	1317
	T20-3	55003	59232	81544	905	1049	1988
Geometry 4	T25-1	55829	56305	70459	1053	1071	1677
	T25-2	49598	53848	84470	854	1007	2477
	T25-3	45295	48231	74074	923	1046	2468
	Average	--	--	--	936	1017	1617
	Standard deviation	--	--	--	62	44	507

Table 4: Experimental G_{IIIC} values from ECT-2 test

The numerical model for ECT-2 test is shown in Figure 9. The simulation allows optimization the position of the sample in the jaws in order to obtain the propagation of the crack. The crack was actually located close to the rotation axes. Then the strain energy release rate along the crack tip calculated by the VCCT method using T_{C-1} value is illustrated by Figure 10. One can see that the conformity of G_{III} with ECT-2 is as good as with MECT-1. In addition, there is much less G_I and G_{II}. However, the numerical average value of G_{III} becomes 20% higher than the experimental one.

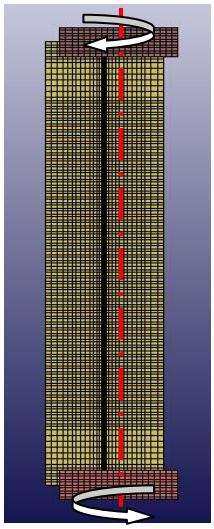

Figure 9: Numerical model of ECT-2

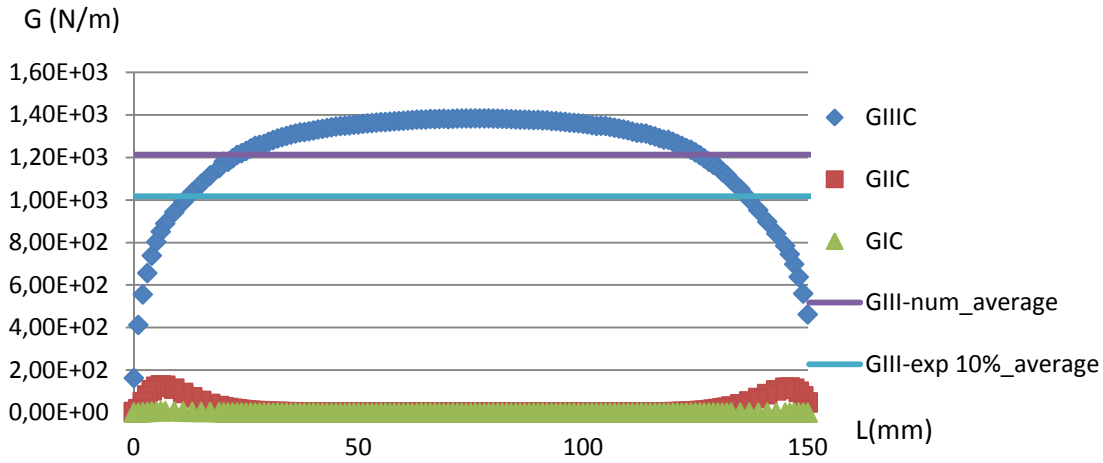

Figure 10: Evolution of G_I, G_{II} and G_{III} along the crack tip in ECT-2 test

4.3. ECRT test

An original test, named Edge-Ring-Crack-Torsion (ERCT) test (Figure 11)[12], is proposed in order to obtain pure mode III delamination. The composite specimen containing a circular crack is maintained by glue to two rigid plates screwed to the torsion devise submitted to torsion.

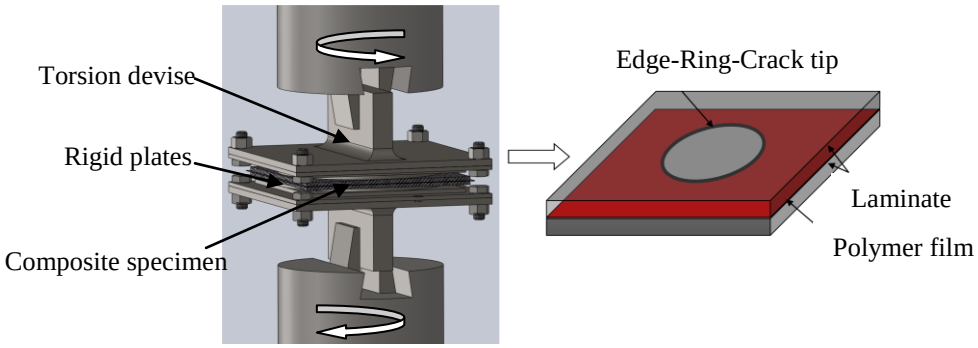

Figure 11: Edge-Ring-Crack-Torsion test configuration

When the specimen is submitted to an imposed torsion, the crack propagates under pure mode III. We observe a sudden drop in the torque as shown in Figure 12, which means the crack propagates in an instable manner.

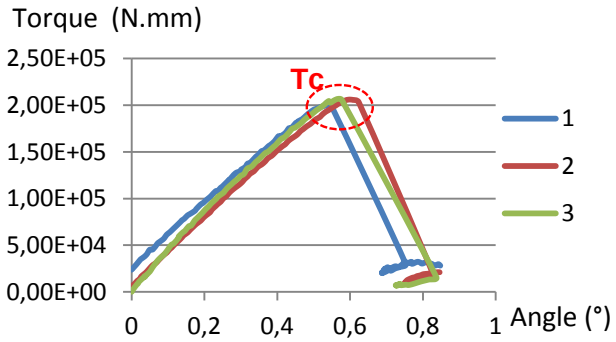

Figure 12: Experimental curves of ERCT test with d=30mm

In the case of a cylinder of diameter D with an external crack of diameter d submitted to a torque T, the stress intensity factor K_{III} is given by a semi analytical equation from Tada Handbook[13] as following:

$$K_{III} = \frac{16T}{\pi d^3}\sqrt{\pi\frac{(D-d)}{2}}.f\left(\frac{\mathrm{d}}{\mathrm{D}}\right) \tag{7}$$

$$f\left(\frac{d}{D}\right) = \frac{3}{8}\sqrt{\frac{d}{D}}.\left[1+\frac{1}{2}\frac{d}{D}+\frac{3}{8}\left(\frac{d}{D}\right)^2+\frac{5}{16}\left(\frac{d}{D}\right)^3+\frac{35}{128}\left(\frac{d}{D}\right)^4+0{,}208\left(\frac{d}{D}\right)^5\right]$$

In fracture mechanics, K_{III} is related to strain energy release rate G_{III} by equation (8) for isotropic materials if the crack growth is in its initial plane (self-similar manner), where G is the shear modulus of the isotropic material.

$$G_{III} = \frac{1}{2G}K_{III}^2 \tag{8}$$

If we calculate the G_{IIIC} according to equations equation (7) and equation (8), we can obtain the results listed in Table 5. It shows that the deviation of G_{IIIC} obtained from different crack diameter is relative small.

d(mm)	D(mm)	$T_{avarage}$(N.mm)	G(MPa)	f	K_{III}(MPa.$m^{1/2}$)	G_{IIIC} (N/m)
30	120	204149	4062	0,2165	3.13	1209
50	120	742147	4062	0,3163	3.17	1239

Table 5: G_{IIIC} obtained from the ERCT tests

The whole torsion device and the composite specimen have been modeled by solid elements and spring elements were inserted at the crack tip.

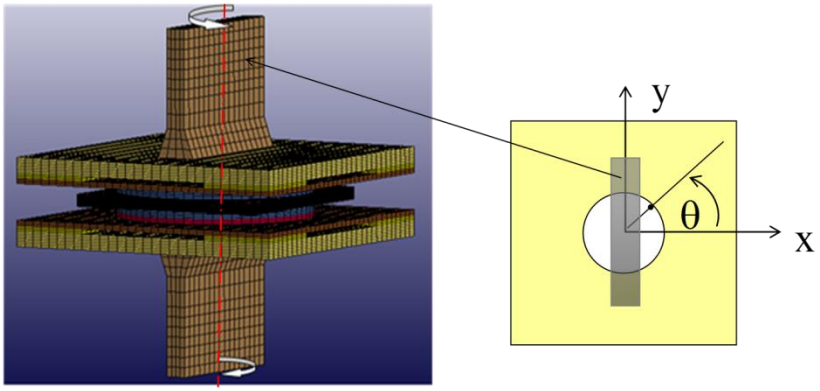

Figure 13: Numerical model of ERCT

As shown in Figure 14 and Figure 15, we obtain quasi pure mode III and G_{II} represents less than 3% of G_{III}.

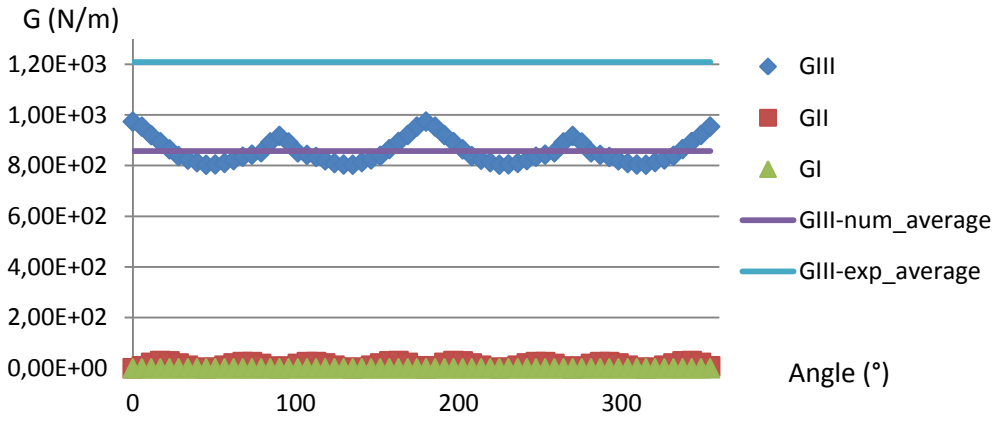

Figure 14: Evolution of G_I, G_{II} and G_{III} along the circular crack front of ERCT test d=30mm

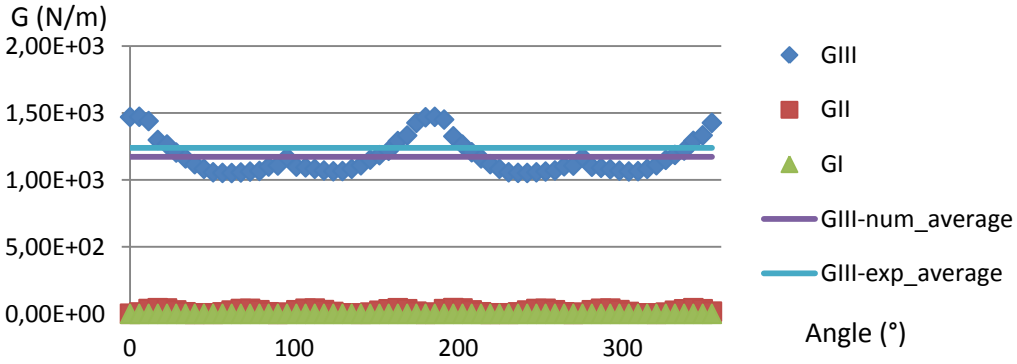

Figure 15: Evolution of G_I, G_{II} and G_{III} along the circular crack front of ERCT test d=50mm

The appearance of 4 wave crests and 4 troughs of G_{III} in Figure 14 and Figure 15 should be caused by stacking sequence and adjacent fiber orientation of the specimen. Moreover the crest values at 0° (360°) and 180° are not identical to the ones at 90° and 270° because of the anisotropy material's response to dissymmetric loading field.

Same models containing cohesive element at crack plane were also established to verify the variation of G_{III}. Material model 186 is applied on the cohesive element, which includes 3 general irreversible mixed-mode interaction cohesive formulations with arbitrary normalized traction-separation law. The results show that the initiation of damage will occur for θ equals 0° or 180° (Figure 16), where G_{III} reaches its maximum according to the results given by models without cohesive elements.

Figure 17 shows the patterns obtained by C-scan on a specimen with the crack of diameter 30mm before and after crack growth. It seems that the crack propagated much more in the direction of adjacent fibers, that means along 0°, 90°, 180° and 270°. These observations are in good concordance with the numerical results shown in Figure 14 and Figure 15.

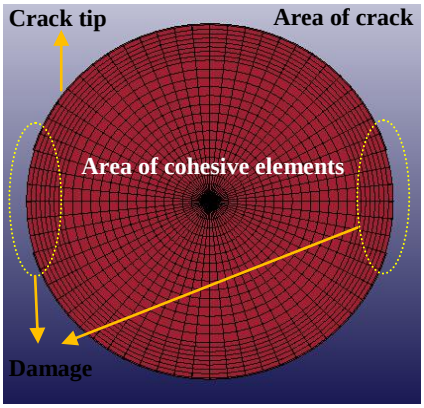

Figure 16: Damage of cohesive element

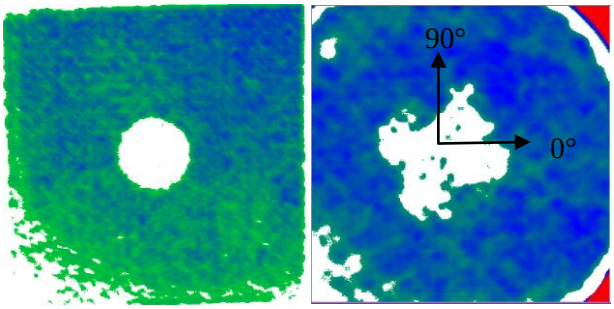

Figure 17: C-scan patterns on a specimen with d=30mm

5. Comparison of G_{IIIC} obtained from different tests and concluding remarks

Table 6 lists the results obtained from different tests.

	G_{IIIC} (N/m) experimental average	G_{IIIC} (N/m) numerical average
ECT-1(a=20)	1310	945
ECT-2(a=20)	926/1005/1774	1213
ERCT d=30mm	1209	857
ERCT d=50mm	1239	1173

Table 6: Comparison of G_{IIIC} determined by different tests

Critical strain energy release rate under pure mode III load is intrinsic to material, but the geometry of specimens and the test configuration seem to influence the measured G_{IIIC} values. The difference between experimental average value and numerical one is not negligible whatever the test configuration. According to experimental average value of G_{IIIC}, ERCT is proved to be less affected by the specimen geometry.

The distribution of G_{III} along crack tip of ERCT specimen is obviously better than that of ECT ones. It varies regularly according to adjacent fiber orientation relative to the crack tip. And it could be improved further if the loading field is axisymmetrical.

Concerning the participation of mode I and mode II, only less than 3% of mode II delamination is found in ERCT while more than 20% is found in ECT tests. We can modify the geometry of ECT specimen to decrease the participation of mode II, but it will never be totally eliminated.

Tests for measuring delamination toughness under pure mode I and mode II loadings were also performed. The results shown in Table 7, demonstrates that delamination behavior in mode II and mode III need to be distinguished considering the difference between G_{IIC} and G_{IIIC}.

Mode	G_{exp}(N/m)	G_{num}(N/m)	Test
I	460	330	DCB
II	914	750	ENF
III	1239	1173	ERCT

Table 7: Toughness of pure mode I, pure mode II and pure mode III

REFERENCES

[1] X.J Gong., Rupture interlaminaire en mode mixte I+II de composites stratifies unidirectionnels et multidirectionnels Verre/Epoxy. *Thèse de doctorat, Université de Technologie de Compiègne*, 1992.

[2] X.J. Gong, M.L. Benzeggagh, Mixed mode interlaminar fracture toughness of unidirectional Glass/Epoxy composite. *Composite Materials: Fatigue and Fracture*, 5, ASTM STP 1230, R.H. Martin, Ed., American Society for Testing and Materials, Philadelphia, 1995, pp. 100-123

[3] S.M.Lee, An edge crack torsion method for mode III delamination fracture testing. *Journal of Composites Technology and Research*, 1993;15(3):193–201.

[4] H.Suemasu, An experimental method to measure the mode III interlaminar fracture toughness of composite laminates. *Composites Science and Technology*, 1999;59:1015-1021

[5] R.Marat-Mendes, M. De Freitas, Characterisation of the edge crack torsion (ECT) test for the measurement of the mode III interlaminar fracture toughness. *Engineering Fracture Mechanics*, 2009;76:2799-2809

[6] P. Robinson, D.Q. Song, A new mode III delamination test for composites. *Advanced Composites Letters*, 1992;1(5).

[7] F. Sharif, M.T. Kortschot, R.H. Martin, Mode III delamination using a split cantilever beam. In: Martin Roderick H, editor. Composite materials: fatigue and fracture—Fifth Volume, ASTM STP 1230. Philadelphia: *American Society for Testing and Materials*, 1995. pp. 85–99.

[8] G.R. Irwin, Fracture I. *Handbuch der Physik*, 1958, pp. 558-590.

[9] E.F. Rybicki, M.F. Kanninen, A finite element calculation of stress intensity factors by a modified crack closure integral. *Engineering Fracture Mechanics*, 1977;9:931-8.

[10] R. Krueger, The Virtual crack closure technique: history, approach and applications. NASA/CR-2002-211628.

[11] R. Marat-Mendes, M. De Freitas, Failure criteria for mixed mode delamination in glass fibre epoxy composites. *Composite Structures*, 2010;92:2292-2298

[12] X.J. Gong, A. Hurez, Y.Y. Ge, L.L. Peng, E. De Luycker, Edge Ring Crack Torsion (ERCT) test for pure mode III toughness. *Proceedings of Journées Nationales sur les Composites (JNC/19), Lyon, France, June 29–July 1; 2015.*

[13] H. Tada, Paris CP, Irwin GR. *The stress analysis of cracks handbook*, 1973

ACKNOWLEDGEMENTS

This work is supported in part by the scholarship from China Scholarship Council (CSC).